Non-contact Low Power EEG/ECG Electrode for High Density Wearable Biopotential Sensor Networks

Yu M. Chi, Stephen R. Deiss and Gert Cauwenberghs
University of California, San Diego
La Jolla, CA 92093
m1chi@ucsd.edu

Abstract—A non-contact capacitive biopotential electrode with a common-mode noise suppression circuit is presented. The sensor network utilizes a single conductive sheet to establish a common body wide reference line, eliminating the need for an explicit signal ground connection. Each electrode senses the local biopotential with a differential gain of 46dB over a 1-100Hz bandwidth. Signals are digitized directly on board with a 16-bit ADC. The coin sized electrode consumes $285\mu A$ from a single $3.3V$ supply, and interfaces with a serial data bus for daisy-chain integration in body area sensor networks.

Keywords-ECG, EEG, Body Sensor, Capacitive Sensing

I. INTRODUCTION

The use of biopotential measurements is an integral tool in both research and clincal settings. Electrical signals on the body's surface like electrocardiograms (ECG), electroencephalograms (EEG), and electromyograms (EMG) provide useful information regarding the physiological state of the subject. Typical recording systems still primarily use wet type electrodes comprised of a metal plate on an adhesive sheet with the skin-electrode interface conducted through a gel paste. Consequently, preparation for each recording is non-trivial and places practical limits on their use for high density, long term, wearable biopotential recording systems.

Capacitive type electrodes that do not require direct contact are attractive in body sensor applications since they require a minimal of preparation and impose the least impact on the end user. Early work [1] [2] have shown efficacy in resolving EEG and ECG type signals through capacitive coupling. Recent developments in microelectronics have revived interest in this type of biopotential sensing.

Prance et. al [3] [4] demonstrated the use of modern integrated amplifiers to achieve the ultra high input impedances necessary to resolve signals through small coupling capacitances. Other contactless sensor approaches [5] [6] [7] have successfully met or exceeded the performance of gel electrodes in ECG applications. However, to date, the full potential of capacitive biopotential sensing in a high spatial resolution wearable body sensor network has not been realized.

In this paper, we present a new active electrode architecture particularly suited for high resolution biopotential sensing. The compact coin sized sensor features a common-mode noise suppression front-end with a high differential gain. A single
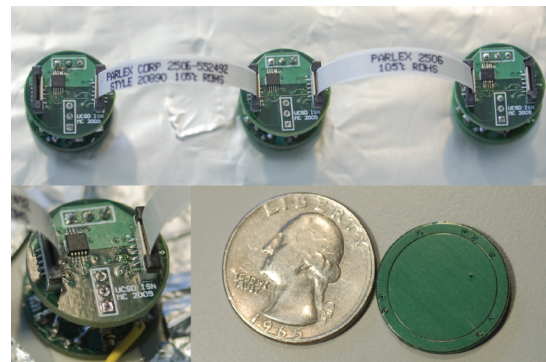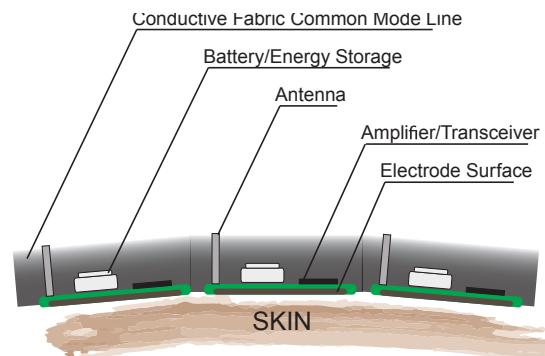

Fig. 1. Wearable biopotential sensor networks monitoring. (Top) Conceptual high-density integration of non-contact biopotential sensors in a wireless body network embedded in conductive fabric, serving as active signal reference. (Bottom) Realized wired network of non-contact sensors, with daisy chain digital output.

conductive sheet, spanning the area of the body being sensed, serves as a common-model signal reference for all sensing nodes, actively driven to the average of each sensor node. Finally, the electrode consumes a minimal of power and has a easy to use fully digital signaling interface.

Fig. 1 illustrates the concept of a fully wireless, non-contact body sensor network for high-resolution biopotential mapping, and the current realization of a wired network with daisy-chain digital readout presented here. This paper focuses on the design of the non-contact sensor with active common-

mode suppression through a single conductive sheet extending over the network. The ability to integrate these networks in lightly conductive fabric make it appealing for non-obtrusive integration in wearable body sensor networks.

II. NON-CONTACT SENSOR DESIGN

A. Electrode Construction

Each sensor (Fig. 1) consists of two small round electrically connected standard printed circuit boards the size of a US nickel coin. The upper board contains a 16-bit analog-to-digital converter and voltage reference. Unlike traditional electrodes that output a single analog signal, interfacing is facilitated through two miniature 10-wire ribbon cables on each side which provides power along with the digital clock, control and data lines.

The ADC output from each board is a serial data stream which is shifted in a daisy chain [8] from board to board to the end of the chain which connects to a custom USB data acquisition interface. This connection scheme minimizes the amount of cabling required across the sensor network, where the total connection length scales with the number of sensors and the average distance between sensors.

Biopotentials are sensed through a $228mm^2$ copper fill insulated by solder mask on the lower board, which is shielded from external noise by the outer copper ring and a solid metal plane directly above the electrode. The amplifier circuit is placed directly on the top surface of the lower board and output an analog signal which is digitized by the upper board.

B. Sensor Amplifier Circuit

Figure 2 shows the analog front-end schematic for a single electrode channel consisting of two operational amplifiers and associated passive components. The first operational amplifier (OA1) provides differential gain and drives the common line. The second operational amplifier (OA2) serves as a buffer to drive the active shield and bootstraps the biasing network.

Biopotentials are coupled to the non-inverting input of OA1 through a capacitance, C_s, formed by the electrode and the skin. For this type of capacitive sensing, the input impedance of the sensor input must be kept extremely high since any finite input resistance forms a high pass filter with the coupling capacitance, shunting the signal. For the low frequencies (0.1Hz-100Hz) in physiological measurements with the small coupling capacitances (0.1-10pF) in non-contact capacitive coupling, the input resistance must be in excess of $1T\Omega$. In addition, it is also desirable to minimize any parasitic input capacitance C_{in}, since it further attenuates the body signal v^i of sensor i in the network as it is received at the amplifier input:

$$v_s^i = \frac{C_s^i}{C_s^i + C_{in}^i}\ v^i. \tag{1}$$

Although the FET input amplifier (LT6078) provides low noise operation at low power consumption with high input impedance and low input capacitance, it requires an input biasing network to provide a DC current path to counteract leakage currents and fix the DC input voltage to a mid-rail level for maximum output signal range. Using a simple resistive bias network is impractical from a reliability and noise standpoint. Although a biasing resistor can be bootstrapped to the required resistance, minimizing its current noise contribution requires an impossibly high value ($> 1T\Omega$). Instead, input biasing was accomplished with two back-to-back diodes to V_{bias} through a $100k\Omega$ resistor, R_b, at DC and provide a path for the amplifier's input bias current in a similar scheme to [3], but with the addition of a second diode for protection and clamping. To mask the diode's parasitic capacitance and conductance, $C_b(2.2\mu F)$ bootstraps the input for input frequencies higher than $1/2\pi R_b C_b$ Hz, thus preserving the amplifier's high input impedance while achieving lower noise levels than what is possible with a purely resistive bias.

Unlike most previous capacitive electrode amplifier designs [3] [4] [7], each electrode serves as a self-contained channel of a distributed biopotential sensor network connected through the common line, V_{cm}, rather than a simple voltage buffer. The output of each electrode is the amplified and filtered difference between the local biopotential, and its spatial and temporal average over the aggregate of electrodes, actively driven and communicated over the shared V_{cm} node.

In each electrode, the non-inverting node of OA1 follows the capacitively coupled signal from the body. This sets V_{cm} to the average of the potentials v_s^i as seen by each electrode, averaged through the passive voltage mixing network formed by R_f and C_f:

$$V_{cm} \approx \frac{1}{N}\sum_{j=1}^{N} v_s^i \tag{2}$$

where N is the number of sensors connecting to the V_{cm} node. The sensor circuit amplifies and filters the difference between v_s^i and V_{cm}, hence performing global common-mode subtraction:

$$v_+^i - v_-^i = A_{fg}(j\omega)\ (v_s^i - V_{cm}) \tag{3}$$

where

$$A_{fg}(j\omega) = \frac{j\omega C_f R_g}{(1 + j\omega R_g C_g)(1 + j\omega R_f C_f)} \tag{4}$$

provides a band-pass response with mid-band gain of $R_g/R_f = 46dB$ over a $1/2\pi R_f C_f = 1Hz$ to $1/2\pi R_g C_g = 100Hz$ bandwidth. For a high resistance fabric used as the common-mode connector, depending on the value of the sheet resistance relative to R_f, the common-mode signal V_{cm} in (2) varies spatially, and the network produces output signals that are spatially as well as temporally high-pass filtered across the sensor array.

For true common-mode components in the input, the current through R_f is zero, so that common-mode signals are absent in the amplified differential signal at the ADC input. Hence, the common mode rejection ratio (CMRR) of the sensor is relatively insensitive to component matching and the amplifier's loop gain. However, the CMRR is critically sensitive to gain variations induced by non-contact capacitive shunting of
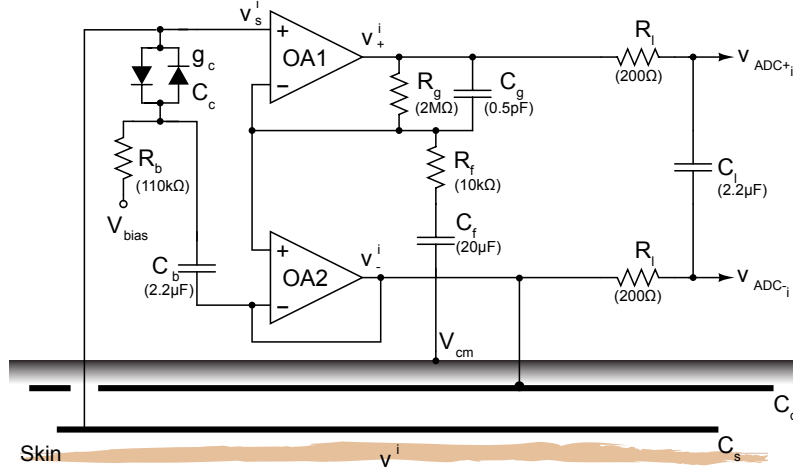
247

Fig. 2. Schematic of electrode analog front end amplifier circuit. All electrodes in the network are joined at V_{cm}, through a single conductive layer spanning the network.

the body signal at the amplifier input. Variations in distance between sensors and the body surface, as well as variations in dielectric properties of texture, cause variations in coupling capacitance C_s that introduce large common-mode gain errors according to (1).

An active shield guards the input from contamination from externally coupled noise. The active shield driven by a buffered version of the input signal has been shown to be effective [4] [6] [9] in guarding the amplifier input without introducing addition loading to the input. Here, the second amplifier, OA2, drives this shield (C_d) and also provides a low-impedance source to drive the differential ADC inputs, with additional anti-aliasing low-pass filtering over $1/2\pi R_l C_l = 100Hz$ bandwidth provided by C_l and R_l.

The net signal at the ADC input, including the effect of noise sources in the amplifiers and input diodes, is approximately given by:

$$V_{ADC}^i = V_{ADC+}^i - V_{ADC-}^i \tag{5}$$
$$= A^i(j\omega)\,(v^i + v_n^i) - \frac{1}{N}\sum_{j=1}^{N} A^i(j\omega)\,(v^j + v_n^j)$$

with net channel gain:

$$A^i(j\omega) = \frac{1}{1 + j\omega R_l^i C_l^i}\,\frac{A_{fg}^i(j\omega)}{1 + \frac{1}{C_s^i}\left(C_{in}^i + \frac{g_c^i(1+j\omega\tau_c^i)}{j\omega(1+j\omega\tau_b^i)}\right)} \tag{6}$$

and with input-referred noise:

$$v_n^i = \frac{C_s^i + C_{in}^i + C_d^i + C_c^i + \frac{g_c^i}{j\omega}}{C_s^i}\,v_{n1}^i$$
$$+ \left(\frac{C_d^i + C_c^i\left(\frac{1+j\omega\tau_c^i}{1+j\omega\tau_b^i}\right)}{C_s^i}\right)v_{n2}^i \tag{7}$$
$$+ \frac{1}{j\omega C_s^i}\,(i_{n1}^i + i_{nb}^i)$$

where v_{n1}^i and v_{n2}^i are the input-referred voltage noise of amplifiers OA1 and OA2 respectively, i_{n1}^i is the input current noise of OA1, and i_{nb}^i is the current noise contributed by the input diodes. The small signal conductance of the double diode input clamp is represented by g_c^i and its associated capacitance by C_c^i. The time constant of the bootstrapped bias network, $\tau_b^i = R_b^i C_b^i$, and the input clamp, $\tau_c^i = g_c^i/(C_{in}^i + C_s^i)$, also appear in the gain and noise expressions.

From the gain equation, the effect of bootstrapping of the input diode serves to mask the diode conductance, g_c, by a factor approximately τ_c^i/τ_b^i as well as canceling its parasitic input capacitance, C_c. This is useful due to the relatively high capacitances associated with the low leakage diodes used for minimizing current noise. It is also desirable to use C_b to minimize the dynamic voltage excursion across the input diode to maintain its low conductance bias point to avoid distorting the signal for larger input swings.

Secondly, while the use of this network largely eliminates the parasitic conductances at the input, it also serves to couple excess voltage noise back to the input node, hence increasing the overall noise levels. Each parasitic shunt conductance at the input node directly increases the net effect of v_{n1}^i by a factor set by the ratio of the the shunt conductance versus the sensor capacitance. The use of the OA2 for shield buffering also couples noise from v_{n2}^i through C_d^i and C_c^i. From a noise perspective, it is still advantageous to minimize each of these parasitic terms, even though feedback and bootstrapping can be used to minimize their impacts on the gain term.

The effect of input current noise, however, is dependent only on the size of the sense capacitance, C_s. For weak sensor coupling, the current noise will dominate the overall noise expression and set the fundamental noise floor for signal detection.

Finally, a source of error is contributed by the C_{in}^i/C_s^i mismatch, resulting in a variable gain reduction from A_{fg} in each channel. For higher gain as well as common mode
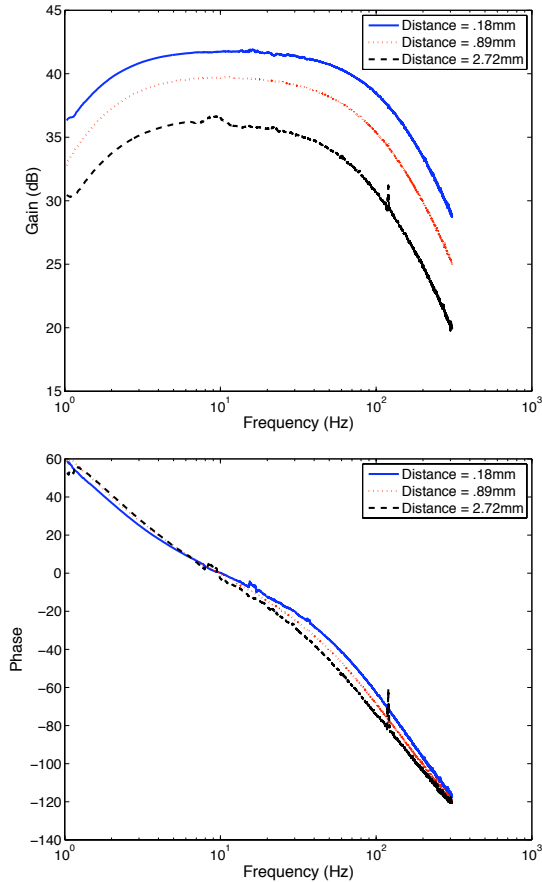
248

Fig. 3. Sensor differential gain (bottom) and phase (bottom) at different distances.

Fig. 4. Sensor input referred noise spectrum at different distances.

rejection, future version will include a compensation network to cancel the effects of amplifier input capacitance.

C. ADC

A 16-bit differential ADC (TI ADS8318) was used to acquire the amplified and filtered signal from the electrode. As previously mentioned, the ADC digital data lines are connected as a daisy chain shifting serial data from the end of the sensor chain back to the host data acqustion module. A common clock and chip select line synchronizes the conversion and transfer of data at a sample rate of $1ksps$.

III. EXPERIMENTAL RESULTS

A prototype network of eight sensors was implemented. All results presented below are obtained with two sensors, implementing two-point differencing. The common mode line is implemented with a single wire.

A. Sensor Gain

Sensor gain is dependent on the ratio of the skin-electrode capacitance versus the parasitic amplifier input capacitance, resulting in decreased gain as the sensor is placed further from
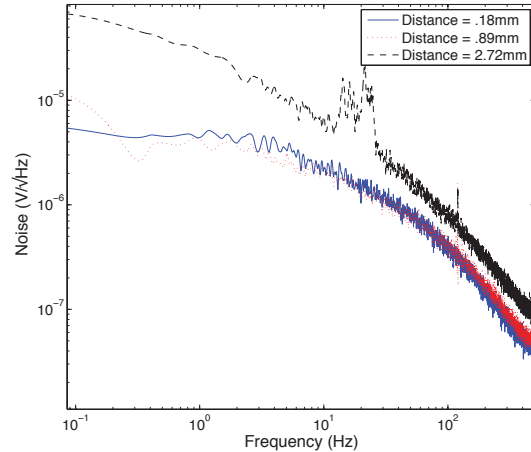
the surface of the skin. To characterize the performance of the sensor at various distances, two sensors were coupled to two metal planes across glass dielectrics of varying thickness.

A differential test frequency sweep was applied to the two metal plates from a function generator. The sensor output, along with the test input were recorded through the ADCs, allowing the gain and phase to be measured.

The gain is shown in Fig. 3 and decreases as the sensor is placed more distant from the signal source, as expected. The phase of the transfer function is virtually invariant over sensor distance, indicating that sensor input has a sufficiently high input resistance that the only signal attenuation is due to the parasitic input capacitance.

B. Noise

Noise levels were measured for a two channel system by placing the two electrodes face-to-face with a glass dielectric of different thickness, thereby shorting the inputs, in a similar manner as before and recording the resultant output noise as measured by the ADC. The input referred noise spectrum is shown in Fig. 4 and is computed by taking the total output noise spectrum and dividing by the previously found mid-band gain at the same separation distance. Total measured in-band input referred noise is approximately $14\mu V_{rms}$ for both the $.18mm$ and $.90mm$ sensor separation distances and degrades significantly for further sensing distances.

Reducing the level of input noise can be accomplished by having a lower input leakage current as mentioned in the previous section. At present, the diodes used have a total leakage current of approximately $6pA$, much larger than the input bias current of the amplifier resulting in $1fA/\sqrt{Hz}$ of current noise. An complete integrated solution with on-chip biasing techniques would significantly improve the noise performance.
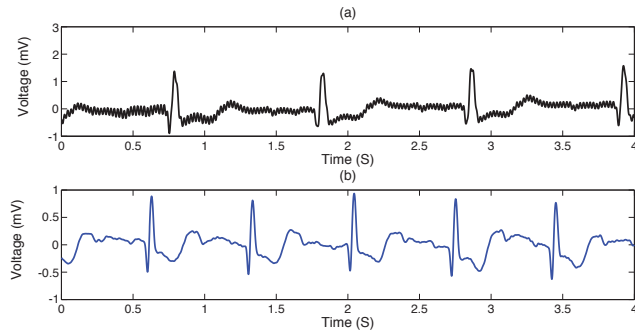
249

Fig. 5. ECG recording taken over subject's chest with non-contact sensor through a cotton shirt (a) and directly over the skin's surface (b). In both cases the signal ground was floating with respect to the body.

C. Power Consumption

Overall power consumption for each electrode including amplifier and ADC is $285\mu A$ at $3.3V$. Power consumption is dominated by the amplifier which consumes a quiescent current of $100\mu A$ for the two device package. This is more than ten times more power efficient than previously reported [9]. The power requirement of only $940\mu W$ at a single $3.3V$ supply along with the fully digital interface makes it easy to interface a large scale network of these electrodes with a low power wireless module or a simple notebook powered USB system.

IV. PHYSIOLOGICAL RECORDINGS

Sample recordings of ECG are shown in Fig. 5 and are made from a two electrode test setup. One sensor was placed above the heart while the second was placed over the opposing rib cage and the differential voltage is recorded. A clear ECG is observed when the sensor is placed directly above the skin's surface. When the recording is made over a shirt, some 60Hz line noise is introduced as a result of capacitive mismatch due to the larger separation distance and corresponding smaller coupling capacitance. Future introduction of an improved active shield that bootstraps the input with gain is expected to significantly reduce the capacitive mismatch common-mode error and eliminate residual line noise.

V. CONCLUSION

A small network of active capacitive electrodes for low-power non-contact biopotential sensing has been implemented and demonstrated. While the effect of capacitive gain errors due to variable strength coupling in non-contact sensing introduces common-mode errors in the received signals, future work involving active bootstrapping is expected to mitigate these effects.

This fully differential amplifier architecture offers several advantages for body wide sensing. First, common mode rejection is handled intrinsically, without the need for an active feedback driven to a reference limb [6]. This allows for the sensor front-end to have a high gain without being susceptible to clipping due to large common-mode noise, maximizing

the noise performance versus a voltage follower [10]. In applications such as wireless networking where the sensor ground is floating, the ability to handle large common mode signals at the front-end is crucial. Secondly, in future body area networks, the entire common-mode line can be manufactured as a conductive fabric sheet which follows the body potential and further shielding the electrodes from external noise.

VI. ACKNOWLEDGMENTS

REFERENCES

[1] A. Lopez and P. C. Richardson. Capacitive electrocardiographic and bioelectric electrodes. *IEEE Transactions on Biomedical Engineering*, 16:299–300, 1969.

[2] P. Park, P.H. Chou, Y. Bai, R. Matthews, and A. Hibbs. A barium-titanate-ceramics capacitive-type EEG electrode. *IEEE Transactions on Biomedical Engineering*, pages 299–300, July 1973.

[3] R.J. Prance, T.D. Clark, H. Prance, and A. Clippingdale. Non-contact VLSI imaging using a scanning electric potential microscope. *Measurement Science and Technology*, 8:1229–1235, August 1998.

[4] C.J. Harland, T.D. Clark, and R.J. Prance. Electric potential probes - new directions in the remote sensing of the human body. *Measurement Science and Technology*, 2:163–169, February 2002.

[5] P. Park, P.H. Chou, Y. Bai, R. Matthews, and A. Hibbs. An ultra-wearable, wireless, low power ECG monitoring system. *Proc. IEEE International Conference on Complex Medical Engineering*, pages 241–244, Nov 2006.

[6] A. Aleksandrowicz and S. Leonhardt. Wireless and non-contact ECG measurement system– the Aachen SmartChair. *ActaPolytechnica*, 2:68–71, June 2007.

[7] T. Maruyama, M. Makikawa, N. Shiozawa, and Y. Fujiwara. ECG measurement using capacitive coupling electrodes for man-machine emotional communication. *Proc. IEEE International Conference on Complex Medical Engineering*, pages 378–383, May 2007.

[8] T.J. Sullivan, S.R. Deiss, T.-P. Jung, and G. Cauwenberghs. A brain-machine interface using dry-contact, low-noise EEG sensors. *Proc. IEEE Int. Symp. Circuits and Systems (ISCAS'2008)*, May 2008.

[9] T.J. Sullivan, S.R. Deiss, and G. Cauwenberghs. A low-noise, non-contact EEG/ECG sensor. *Proc. IEEE Biomedical Circuits and Systems Conf. (BioCAS'2007)*, November 2007.

[10] E.S. Valchinov and N.E. Pallikarakis. An active electrode for biopotential recording from small localized biosources. *Biomedical engineering Online*, 3, July 2004.